Journal of Porous Materials (2019) 26:1507–1521
https://doi.org/10.1007/s10934-019-00748-4

Fe(III) porphyrin metal–organic framework as an artificial enzyme mimics and its application in biosensing of glucose and H_2O_2

Morvarid Aghayan[1] · Ali Mahmoudi[1] · Khodadad Nazari[2] · Saeed Dehghanpour[3] · Samaneh Sohrabi[3] · Mohammad Reza Sazegar[1] · Navid Mohammadian-Tabrizi[4]

Published online: 29 March 2019

Abstract

Metal–organic frameworks with diverse structures and unique properties have demonstrated that can be an ideal substitute for natural enzymes in colorimetric sensing platform for analyte detection in various fields such as environmental chemistry, biotechnology and clinical diagnostics, which have attracted the scientist's attention, recently. In this study, a porous coordination network (denoted as PCN-222) was synthesized as a new biomimetic material from an iron linked tetrakis (4-carboxyphenyl) porphyrin (named as Fe-TCPP) as a heme-like ligand and Zr_6 linker as a node. This catalyst shows the peroxidase and catalase activities clearly. The mechanism of peroxidase activity for PCN-222 was investigated using the spectrophotometric methods and its activity was compared with the other nanoparticles which, the results showed a higher activity than the other catalysts. Also, the hydrogen peroxide was detected by PCN-222(Fe) based on the peroxidase-like activity. For detection of hydrogen peroxide a linear range of 3–200 μM and detection of limit (LOD) 1 μM (3σ/slope), under optimal conditions were obtained. Moreover, based on the high tendency of PCN-222(Fe) to combine with the TMB as a chromogenic substrate in the peroxidase-like activity, we developed the sensitive and selective colorimetric assay for glucose detection that was found a detection limit (LOD) of 2.2 μM in the linear range from 12 to 75 μM. Finally due to the good catalytic activity of PCN-222(Fe), it was used to detection of glucose and hydrogen peroxide in real samples.

✉ Ali Mahmoudi
mahmoudiali.ac@gmail.com

[1] Department of Chemistry, Faculty of Science, North Tehran Branch, Islamic Azad University, Tehran, Iran

[2] Research Institute of Petroleum Industry, N.I.O.C, Tehran, Iran

[3] Department of Chemistry, Faculty of Science, Alzahra University, Tehran, Iran

[4] Department of Chemistry, Faculty of Science, University of Tehran, Tehran, Iran

Graphical abstract

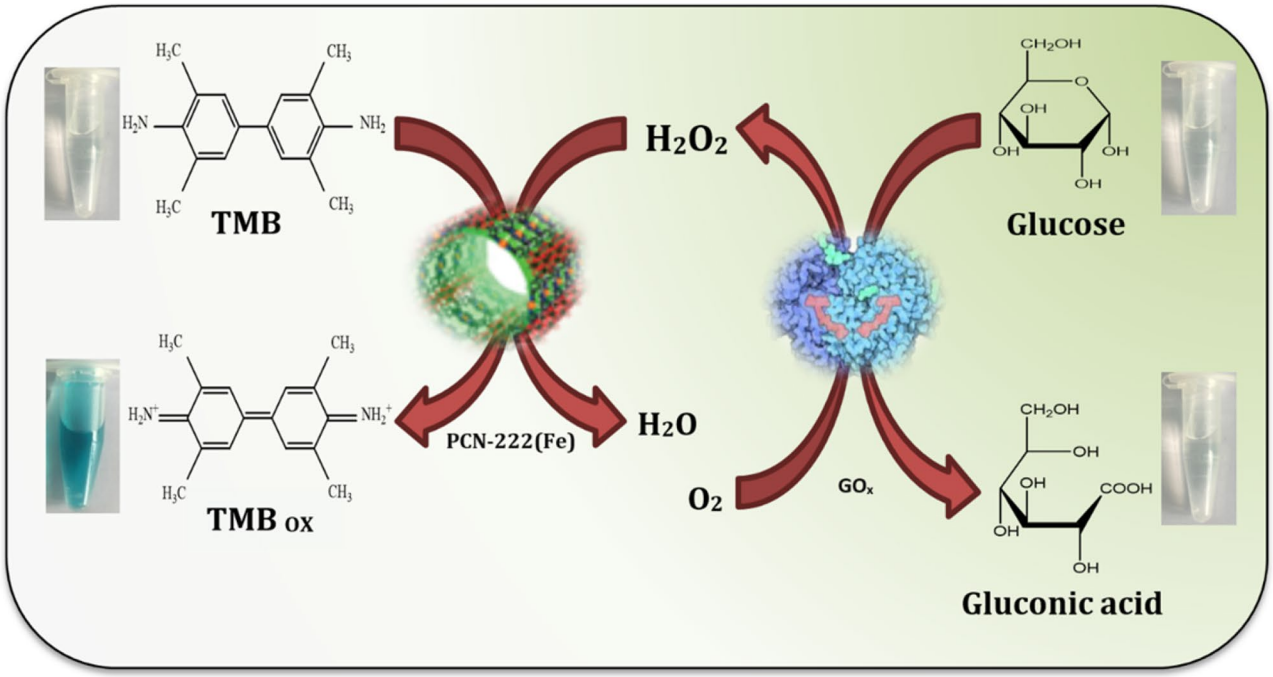

Keywords Metal–organic frameworks · PCN-222(Fe) · Nanozyme · Enzyme mimetic · H_2O_2 detection · Glucose detection

1 Introduction

Nowadays, sensors have attracted significant attention as one of the most effective and precise options for controlling the factors that affect biological processes [1, 2]. Many researches have proven the application of sensors as a sensitive tool in the quantitative and qualitative detection of materials in various fields such as the medical, industrial and environmental [3–5]. Construction of sensors for detection of glucose and H_2O_2 are good examples of notable and valuable topics in this field [6, 7]. Glucose is one of the principal and essential sources in the human body that supplies the energy of living cells and metabolic intermediates [8]. Detection of this substance is vital in clinical diagnosis [9]. Excessive glucose is one of the main causes of development of many diseases such as diabetes [10]. Also, H_2O_2 is one of the common compounds in the production of active oxygen species [11]. Monitoring of this oxidant is indispensable because there is a byproduct of many chemical and biological reactions [12]. Various methods were developed in detection systems by developing the first glucose sensor [13] such as spectrophotometric [14], electrochemical [15–17], and spectrofluorescence techniques [18].

In recent years, sensors based on enzymatic reactions are more significance in research. These sensors have unique features that can be noted to their high ability to direct, selective, and sensitive determination of various compounds, also continuous and very fast control of metabolic activity and lack of side effects [19, 20]. Peroxidase enzyme is more common than other enzymes used in this field. This enzyme causes the oxidation of many organic and inorganic substrates and, like other natural enzymes, has inherent problems such as, dependence on environmental conditions, low stability and high cost [21–23]. A new perspective on biomimetic chemistry has emerged with designing of the Fe_3O_4 nanoparticles (NPs) that showed an intrinsic peroxidase mimetic activity [24]. So far, many substitutes have been designed with imitate the structure and function of peroxidase that are very stable and inexpensive [25]. CO_3O_4 NPs [26], V_2O_5 nanowire [27], FeS [28], graphene oxide [29], carbon nanodots [30] and metal–organic framework (MOFs) [31] are remarkable example. Metal–organic framework (MOFs) is a new platform in artificial enzymes with crystalline, porous and stable structures, and also unique singularities such as high surface area, low density and large pore aperture [32–34]. The potential internal porosity that the guest molecule can reach the pores is the most important feature of MOFs for catalytic and measuring purposes [35]. Notable examples of these super molecules have been discovered. Such as

MOF-525 [36], MMPE-6 [37], CHF-1 [38], MIL-53 [39] and MIL-100 [40].

Metal–organic frameworks (MOFs), also known as porous coordination networks (PCNs). PCN-6 is the first member of the series that were identified in 2006. This collection has been identified new members that some of them include: PCN-224, PCN-229, PCN-600 [41, 42]. Zhou and coworkers have synthesized MOFs based on metalloporphyrin denoted as PCN-222. PCN-222 has Fe-TCPP (tetrakis 4-carboxyphenyl porphyrin) as a heme-like ligand and highly stable Zr_6 as nodes for the assembly of stable Zr-MOFs [43]. The general characteristics of most of PCNs can be noted: (i) following the ping-pong mechanism (ii) having initial peroxidase mimetic [44].

This is a deep and extensive research on the PCN-222(Fe) for evaluation of its peroxidase-like activity and catalase-like activity through appropriate kinetic models. Kinetic constants (k_m, V_{max}, k_{cat}, Cat_{eff}) were determined using Michaelis–Menten, Line-weaverburk and Eadie-hofstee graphs. Results were obtained with TMB as substrate and compared with horseradish peroxidase (HRP) and other peroxidase model compounds. Based on this finding, we have developed a novel platform for colorimetric detection of H_2O_2 and glucose, Also the prepared catalyst was used for biosensing of glucose in biological samples.

2 Experimental

2.1 Materials

All chemicals were used of analytical grade and used as received without further purification. Methyl-4-formylbenzoate, pyrrole, propionic acid, N,N-dimethylformamide (DMF), N,N-diethylformamide (DEF), acetone, $FeCl_2{\cdot}4H_2O$, $ZrCl_4$, Horseradish peroxidase (EC 1.11.1.7), H_2O_2 solution (30% aqueous), were purchased from Merck Chemical Co (Darmstadt, Germany). 3,3′,5,5′-tetramethylbenzidine (TMB), glucose oxidase (GO_x) were obtained from Sigma Aldrich Chemical Co. Glucose, fructose, maltose, galactose and other chemical reagents were obtained from Across Chemical Co. All solutions were prepared using deionized water (Barnstead Nano Pure D8992 deionizer, electrical resistance = 18 MΩ).

2.2 Methods

SEM images were recorded by using a LEO 1455VP operated at an acceleration voltage of 10 kV. The pore morphology of the samples was investigated by TEM imaging on a Zeiss-EM10C-100 KV. Infrared (IR) samples were prepared as KBr pellets, and their spectra were obtained on a Bruker Tensor 27 spectrophotometer. X-ray powder diffraction (XRD) patterns of the sample were recorded on a PHILIPS PW 1800 X-ray powder diffractometer with a CuK_α line (1 = 1.54060°A) as the incident beam. XPS was carried out by using a Gamma data-scienta ESCA200 hemispherical analyzer equipped with an AlKa X-ray source (1486.6 eV) with a monochromator. Electronic spectra and kinetic experiments were obtained by using a UV/Vis a double beam Cary-100 spectrophotometer.

2.3 Synthesis of FeTCPPCl

FeTCPPCl was prepared according to a procedure described previously in three steps as follows [45, 46] .

2.3.1 5,10,15,20-Tetrakis(4-methoxycarbonylphenyl)porphyrin (TPPCOOMe)

Pyrrole (43 mmol, 3.0 mL) was added dropwise to a solution of methyl p-formylbenzoate (42 mmol, 6900 mg) in propionic acid (100 mL). Resulting solution was refluxed for 10 h. Upon cooling to room temperature the precipitates were appeared, in which collected by filtration and washed with methanol, ethyl acetate, and THF. After drying in an oven, a purple solid was obtained as the pure product (1.9 g, 2.24 mmol, 21% yield).

2.3.2 [5,10,15,20-Tetrakis(4-methoxycarbonylphenyl)-porphyrinato] iron(III) chloride ([TPP-COOMe]$Fe^{III}Cl$)

A mixture of TPP-COOMe (1 mmol, 854 mg), $FeCl_2{\cdot}4H_2O$ (12.8 mmol, 2500 mg) and DMF (100 mL) was heated to reflux for 6 h. Mixture was cooled to room temperature then water (150 mL) was introduced. The resulting precipitate was collected by filtration and washed with H_2O (50 mL) twice. Final solid dissolved in $CHCl_3$ and washed three times with 1 M HCl and water. The organic layer was then dried over anhydrous magnesium sulfate and evaporated to give a quantitative yield of dark brown crystals.

2.3.3 [5,10,15,20-Tetrakis(4-carboxyphenyl) porphyrinato] iron(III) chloride (FeTCPPCl)

The obtained ester (750 mg) was stirred in THF (25 mL) and MeOH (25 mL), and a solution of KOH (46 mmol, 2630 mg) in H_2O (25 mL) was added. The mixture was heated to reflux for 12 h. After cooling to RT, THF and MeOH were evaporated. Water was then added to the resulting water phase, and the mixture was heated until the solid was dissolved fully. Solution was acidified with 1 M HCl until no further precipitate was appeared. The brown solid was collected by filtration, washed with water, and dried in vacuum. FTIR (KBr): $\bar{\upsilon}$ = 3447 (m), 3050 (w), 2650 (w), 1694 (s), 1604 (s),

1560 (m), 1402 (s), 1300 (m), 1268 (s), 1201 (m), 1174 (m), 1102 (m), 999 (s), 866 (m), 796 (s), 765 (s), 717 cm^{-1} (m).

2.4 Synthesis of MOF (Fe)

PCN-222 was prepared according to a method reported previously by Feng [43, 46]. $ZrCl_4$ (0.32 mmol, 75 mg), FeTCPPCl (0.056 mmol, 50 mg), and benzoic acid (220 mmol, 2700 mg) in DEF (8 mL) were dissolved ultrasonically in a 20 mL Pyrex vial. The vial was heated in an oil bath at 120 °C under stirring with a stir bar for 24 h. After cooling to RT, a dark brown powder was obtained by centrifugation. FTIR (KBr): $\bar{\upsilon}$ =3444 (m), 2980 (w), 1691 (w), 1603 (s), 1557 (s), 1417 (vs), 1326 (s), 1178 (m), 1000 (s), 871 (w), 804 (m), 770 (m), 712 cm^{-1}(s).

2.5 Activation of the MOF (Fe)

To remove the unreacted starting materials and trapped benzoic acid, as-synthesized PCN-222 (~ 100 mg) was immersed in DMF (40 mL) at 120 °C for 12 h. Afterwards, the sample was centrifuged and washed with DMF and acetone. Fresh acetone was added, and the sample was maintained for 24 h. Finally, the extract was decanted carefully and dried under vacuum for 6 h.

2.6 Biocatalyst assays and kinetics

Peroxidase and catalase-like activity of PCN-222(Fe), were followed and measured spectrophotometrically by collecting absorbance—time data for reactant or product of the reaction (Fig. 1). Spectrophotometric measurements and progress curves were obtained using a double beam Cary-100 spectrophotometer equipped with temperature control accessory.

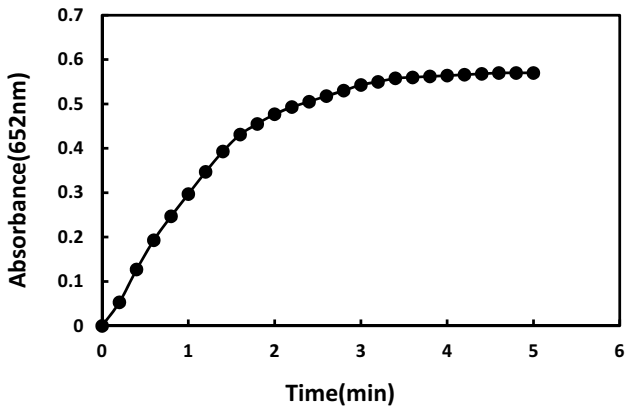

Fig. 1 Typical progress curve for oxidation of TMB by PCN-222(Fe). [TMB] = 0.1 mM, [H_2O_2] = 0.5 mM, PCN-222(Fe) = 2.5 µM, pH 4.0, T = 20 °C

To evaluate the reproducibility and accuracy of the results, each experiment is repeated for 3 times.

The results were evaluated by fitting data to the Michaelis–Menten Eq. (1):

$$V = \frac{V_{\max}[S]}{K_m + [S]} \tag{1}$$

The Michaelis–Menten constant was calculated using Lineweaver–Burk plots of the double reciprocal of the Michaelis–Menten Eq. (2) [47]:

$$\frac{1}{V} = \frac{K_m[S]}{V_{\max}[S]} = \frac{K_m}{V_{\max}}\frac{1}{[S]} + \frac{1}{V_{\max}} \tag{2}$$

where V is the rate of conversion, V_{max} is the maximum rate of conversion, $[S]$ is the substrate concentration, and K_m is the Michaelis constant.

In order to confirm the kinetic parameters obtained from Lineweaver–burk, the Eadie–Hofstee diagrams was also used. In Enzymology, an Eadie–Hofstee diagram is a graphical representation of enzyme kinetics in which reaction velocity is plotted as a function of the velocity vs. substrate concentration ratio [48]. Equation (3):

$$V = -K_m\frac{V}{[S]} + V_{\max} \tag{3}$$

2.7 Peroxidase—like activity

To verify the compliance of the Michaelis–Menten kinetic mechanism upon the peroxidatic activity (peroxidase mimicking) of the nanocatalyst enzyme model, PCN-222(Fe), assays were performed by following concentration of TMB as the chromogenic hydrogen donor substrate at a fixed concentration of H_2O_2. Experiments were carried out using 2.5 µM PCN-222(Fe) in a reaction volume of 930 µL acetate buffer solution (50 mM, pH 4.0, T = 25 °C), 0.5 mM H_2O_2 and at various concentrations of TMB. Absorbance changes of the peroxidatic reaction product, oxidized TMB, were followed and recorded at 652 nm. An extinction coefficient of $\varepsilon = 3.9 \times 10^4\ M^{-1}\ cm^{-1}$ was used to calculate the product concentration of TMB [49]. For the direct determination of concentration of H_2O_2, a molar absorptivity of $\varepsilon = 43.6\ mM^{-1}\ cm^{-1}$ was used [49].

2.8 Catalase—like activity

To evaluate catalase-like behavior of PCN-222(Fe), depletion of H_2O_2 was investigated in the presence of TMB. A typical experiment of catalase activity was carried out using 2.5 µM PCN-222(Fe), 0.1 mM TMB at varied concentrations of H_2O_2 substrate.

2.9 H_2O_2 detection

In a typical experiment, (a) 20 µL of 5.0 mM TMB, 32 µL of PCN-222(Fe) stock solution and 100 µL H_2O_2 of different concentrations were added into 950 µL of 50 mM acetate buffer (pH 4.0) (b) after mixing, the solution was incubated in 25 °C for 10 min (c) absorbance changes of the resulting reaction mixture was measured by using spectrophotometer at λ = 652 nm.

For demonstrating of the sensitivity and selectivity of PCN-222(Fe) as a sensor in H_2O_2 detection, we applied milk as a real sample. At first the sample was firstly centrifuged to remove the organic substances such as protein, fat and so on, then the solution was diluted three fold and was applied for the same detection steps as mentioned above.

2.10 Glucose detection

Glucose detection was carried out as follows: firstly, 0.1 mL of GO_x aqueous solution (3.0 mg mL^{-1}) and 100 mL of D-glucose with various concentrations were mixed and incubated at 37 °C for 30 min, then 0.02 mL of TMB(8 mM) ,0.032 mL of PCN-222(Fe) stock solution, and 760 µL of acetate buffer (50 mM, pH 4.0) were successively added to the glucose reaction solution; finally the mixed solution was incubated at for 15 min for standard curve measurement. To examine the specificity of the method in present of the assay, 5 mM maltose, fructose, galactose instead of glucose were used as controls.

In order to demonstrate glucose concentration in the real serum samples, the serum samples from the local hospital were firstly treated by centrifugation at 10,000 rpm for 30 min to eliminate large aggregates in human serum. The serums were diluted 100 times with phosphate buffer (PBS, 50 mM, pH 7.0) before measurements, then 100 µL suitable concentration of diluted serums were used with GO_x for glucose determination as the same steps above and the corresponding absorbance was measured at a wavelength of 652 nm.

3 Results and discussion

3.1 Characterization of PCN-222(Fe)

Description and Characterization of PCN-222(Fe) as catalyst: PCN-222 is a catalyst which has all the essentials for a heterogeneous catalyst showing enzyme like behavior: possessing porphyrinic catalytically active moieties, large pore size, and high stability in aqueous systems. Each porphyrin containing active center may be regarded as a nanoreactor.

The porphyrin-based metal organic framework with 3D channels was synthesized solvothermally from $ZrCl_4$ and FeTCPP. The structure and morphology of MOF were investigated using UV/Vis spectroscopy, SEM, TEM, XRD, XPS and Infrared data.

The absorption spectra of TPPCOOMe, [TPP-COOMe]$Fe^{III}Cl$, PCN-222 are given in (Fig. 2a). TPPCOOMe spectra shows the Soret band (second exited state) and Q bands (lowest excited state) at λ = 419 nm and λ = 514, 549, 589, and 646 nm, respectively. The UV/vis spectrum

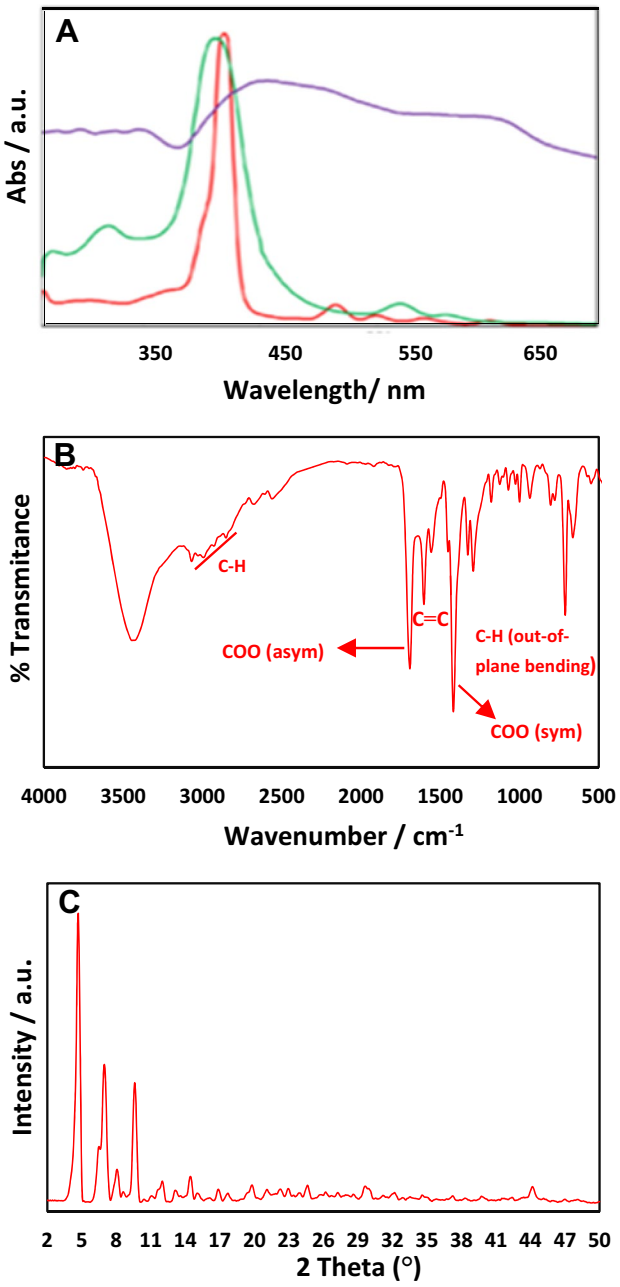

Fig. 2 **a** UV/Vis absorption spectra of TPPCOOMe (1.20 mg L^{-1}; red), [TPPCOOMe]$Fe^{III}Cl$ (1.7 mg L^{-1}; green), PCN-222 (5.6 mg L^{-1}; purple). **b** FTIR spectra of PCN-222(Fe); **c** XRD patterns of PCN-222(Fe)

of [Tpp-COOMe]$Fe^{III}Cl$ shows the blue shift of the Soret band at λ = 414 nm and a decreased number of Q bands (λ = 570 and 609 nm). Based on Gouterman, Iron (III) porphyrins belong to the d-type hyper porphyrins that have hole in the e.g. (dπ) orbitals and they display ligand to metal charge transfer transitions [50]. For PCN-222, part of the Soret band along with broadening can be observed.

FTIR spectra of PCN-222 is shown in (Fig. 2b). The strong stretching vibrations of COO (asymmetric) and COO (Symmetric) are observed at ῡ = 1691 and 1417 cm^{-1}, respectively. The other peaks at ῡ = 2920–3090 (C–H bond of the benzene and pyrrole ring), 1557–1603 (C=C phenyl and pyrrole), and 1326 cm^{-1} (pyrrole deformation) confirm the direct incorporation of the porphyrin in networks. The peaks at ῡ=712 and 804 cm^{-1} are assigned to C-H (out-of plane bending of the phenyl rings) [51, 52].

XRD patterns of PCN-222 are presented in (Fig. 2c). Most peaks are observed in the small angle region due to the mesoporous nature of PCN-222. This is in agreement with data reported previously for PCN-222 [45] .

The XPS spectra of PCN-222 is shown in (Fig. 3A). PCN-222 indicates C 1s, N 1s, O 1s, Zr 3p and Zr 3d. The high resolution spectra of $Fe2p_{3/2}$ and N1s of iron porphyrins located in 3D MOF structure can be observed in (Fig. 3B) The binding energy of 711.5 eV is attributed to the presence of Fe^{+3} inside the porphyrin core and that of 398.9 eV is assigned to N of Fe–N bond.

SEM image revealed that PCN-222(Fe) is composed of uniform Needle-shaped crystals (Fig. 4a). TEM result for

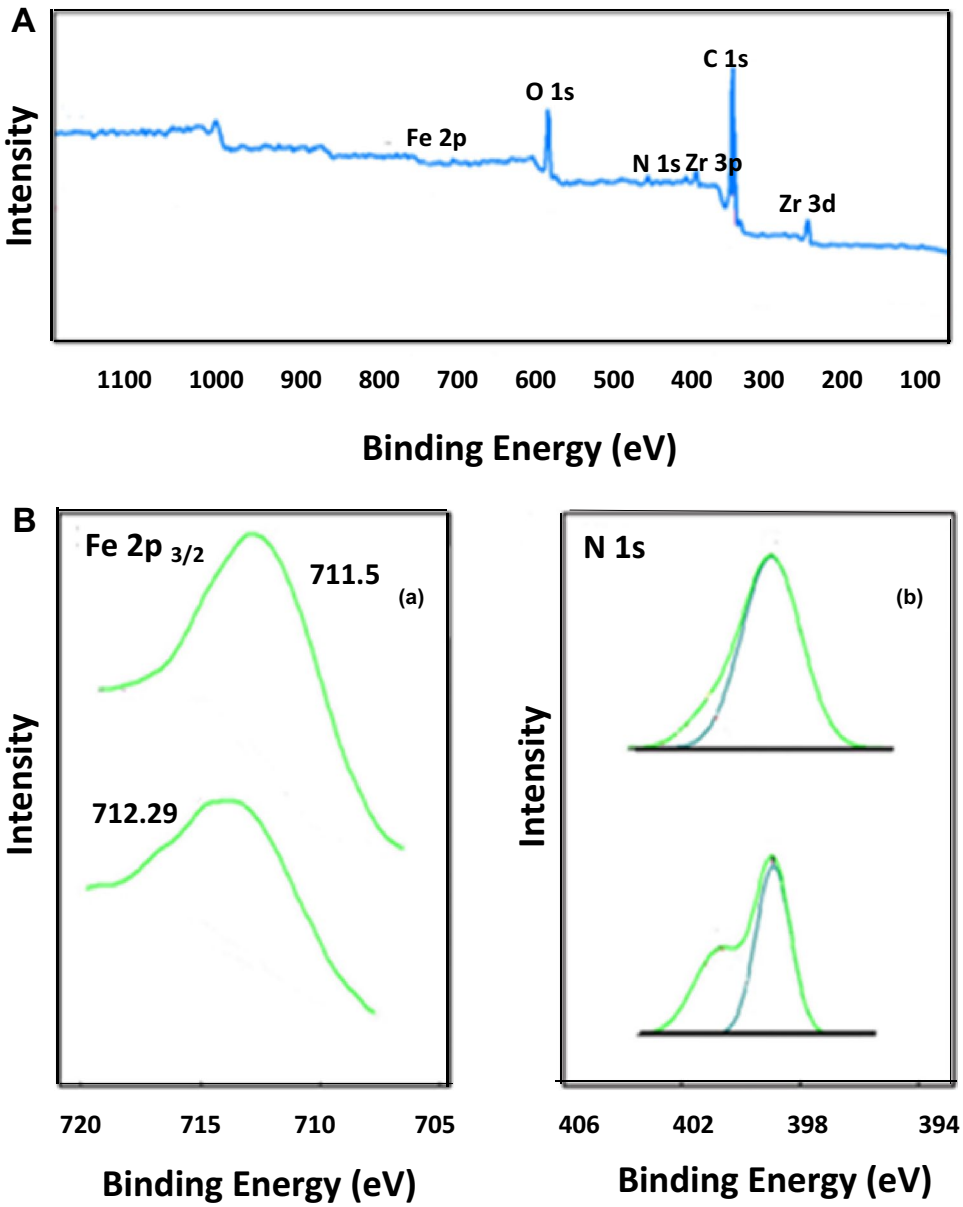

Fig. 3 **A** XPS spectra of PCN-222 and **B** (*a*) $Fe2p_{3/2}$ core-level XPS spectra of PCN-222 (*b*) N1s core-level XPS spectra of PCN-222

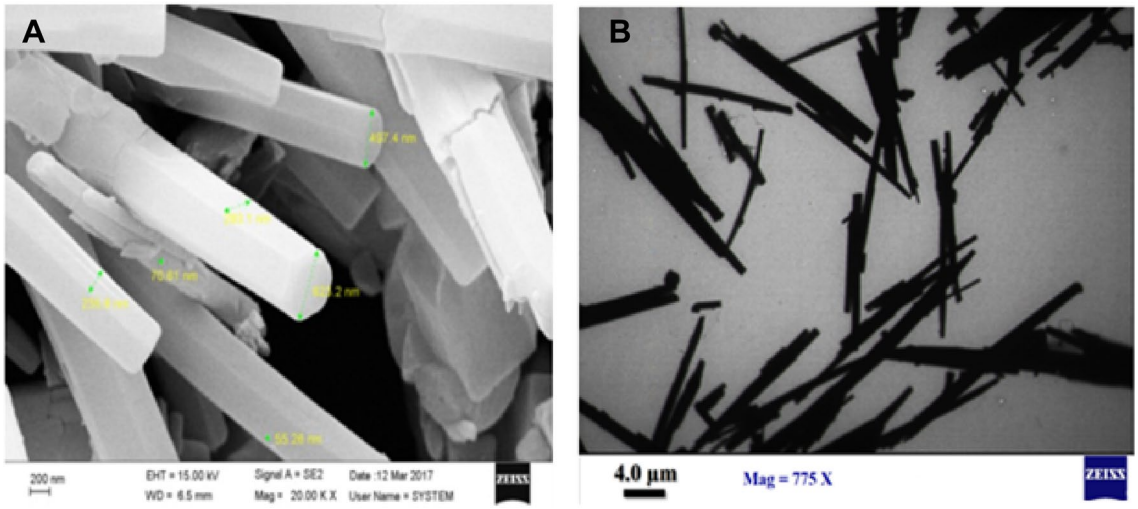

Fig. 4 **a** SEM image of PCN-222 and **b** TEM image of PCN-222

PCN-222 is in agreement with the results and data obtained from XRD analysis and patterns (Fig. 4b).

Compared to metalloporphyrins encapsulated in porous media which suffer from aggregation, metalloporphyrins in PCN-222(Fe) acts a linker attaching Zr_6 clusters (as a node) together yielding an evenly distributed catalytically centers [53]. Such centers behave quietly similar to active sites of heme-containing enzymes in terms of facile diffusion and transportation of substrates. So we expect enhanced kinetic parameters. The 3-D robust structure of PCN provides magnificent stability. Contrary to enzymes thermal stability and chemical stability of PCN-222(Fe) against industrial reaction condition would be improved [54].

3.2 Evaluation of catalytic performance

Considering that PCN-222(Fe) has porphyrin rings and these rings functions similar to the active site of peroxidase (horseradish peroxidase).The PCN-222(Fe) like the other nanozymes can be used to catalyze the oxidation of several organic substrates such as o-methoxyphenol(guaiacol), 2,2′-azino-bis 3-ethylbenzthiazoline-6- sulfonic acid (ABTS) and 3,3′,5,5′-tetramethylbenzidine (TMB) [55] .

Here we selected TMB as a chromogenic substrate to study peroxidase model in presence of H_2O_2 by PCN-222(Fe). A typical experiment of peroxidase activity was carried out using 2.5 µM PCN-222(Fe), 0.5 mM H_2O_2 at varying concentration of TMB. The reaction mixture was homogenized by sonication for 1 min followed by recording the absorbance change by spectrophotometer at 652 nm (Fig. 5 inset). As (Fig. 5 inset) illustrates the mechanism of oxidation reaction of TMB is completed within 5 min. The initial rate was calculated by measuring the slope of the linear region of this curve and then by benefit from initial rate, other kinetic parameters were

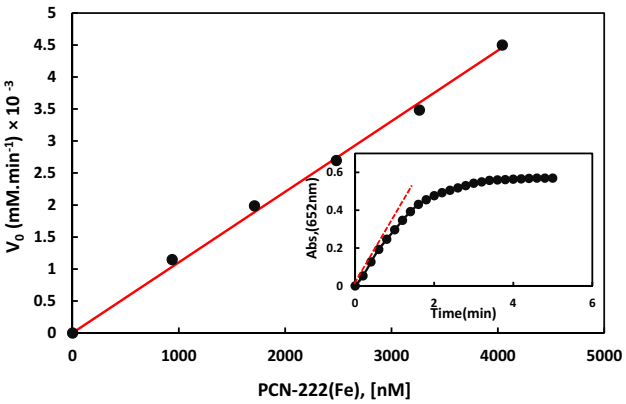

Fig. 5 Initial reaction rates for the oxidation of TMB substrate as a function of amount of PCN-222(Fe) catalyst. Reactions were carried out in the presence [TMB] = 0.2 mM, [H_2O_2] = 0.5 mM, using different amounts of the catalyst. (inset) UV–vis absorbance-time curves of reaction systems catalyzed by PCN-222(Fe) using TMB as chromogenic substrates and H_2O_2

determined. It can be seen that PCN-222(Fe) as a catalyst, mimics peroxidase behavior in the oxidation reactions and also to evaluate, check and finally estimate the kinetic rate constants (k_1,k_3) in following Eq. (4), Initial reaction rate variation against catalyst concentration was investigated [56] :

$$\text{Rate} = \frac{dx}{dt} = \frac{[\text{catalyst}]}{(1/k_1[H_2O_2] + (1/k_3[S]_0))} \quad (4)$$

where [S] is the reductant (aromatic) substrate, k_1 is the velocity constant of the reaction of peroxidase model with hydrogen peroxide resulted in production of compound I species (a πradical cation oxoferryl species) and k_3 represents the velocity constant of conversion of compound

II species to the resting state of the heme enzyme model. k_1 and k_3 can be obtained by fitting the experimental data shown in (Fig. 5) into Eq. (4) (Table 1).

3.3 The peroxidase/catalase like activity of PCN-222(Fe)

Multifunctional activity of peroxidases towards various biosynthetic transformations is of paramount importance. This can be implied by the diverse functional roles of peroxidase isozymes [57], so that important reaction routes and transformations including: (1) Oxidative dehydrogenations, (2) Oxygen transfer reactions, (3) Oxidative halogenations, (4) H_2O_2 disproportionation [58] in the aqueous and organic media become potentially feasible. For example, isolation of a functional hemoenzyme capable of simultaneous high catalytic ($H_2O_2 + H_2O_2 \rightarrow 2H_2O + O_2$) and peroxidatic activity ($H_2O_2 + 2AH_2 \rightarrow 2H_2O + 2\,^{\bullet}AH$) has been an important finding [59].

Any heme enzyme active site consists of a heme prosthetic group (iron–protoporphyrin IX) which has the best possible natural design, micro-environment and specificity toward the substrate and the reaction to be catalyzed [60]. The main heme access channel allows H_2O_2 (as the first substrate) to reach the heme iron for activating the enzyme to a strong oxidant specie referred to as, Compound I [61, 62].

For industrial purposes, modified peroxidases are good choices because of their higher operational stability and activity. Such modification may include the following strategies and approaches: rational design, directed evolution, and replacement of the native heme prosthetic group (reconstitution) [63]. However, the complexity and high cost of such techniques together with low stability of the native peroxidases, limits their applications in real and large scale industrial processes. To overcome these limitations, artificial or natural-based heme-peptides known as mini-peroxidases have been examined as alternative hemoenzyme models, particularly microperoxidases (MPs 8, 9 and 11) derived from proteolytic digestion of Cytochrome C [64]. Synthetic and natural iron(III) porphyrins can also play such a role but at a lower efficiency and higher exposure and vulnerability of the heme group. The chemistry and mechanism of peroxide activation of heme compounds (hemoenzymes, miniperoxidases and heme complexes) through heterolytic cleavage of H_2O_2 have been extensively investigated and reported [65].

In order to have an efficient oxidation process, the substrate might have easy access to the iron of the porphyrin complex in a geometry that facilitates the electron transfer phenomenon. In peroxidases, substrate discrimination is controlled by the protein backbone near the active site while in iron porphyrin complexes, such a substrate specificity at the accessible distal and proximal sites cannot be expected [66] .

For our catalyst, PCN-222, porosimetry studies reveals the presence of two types of pores, with sizes of 1.3 nm and 3.2 nm and a Brunauer–Emmett–Teller (BET) surface area of 2200 m^2g^{-1}. Such large surface area offers large channels with accessible catalytic sites for the substrates, which greatly facilitates their diffusion [45].

Peroxidase like activity of PCN-222 was evaluated through oxidation of the peroxidase substrate, 3,3′,5,5′-tetramethylbenzidine (TMB), in the presence of H_2O_2. During the reaction, TMB substrate transformed into a blue color product with maximum absorbance at 650 nm (Fig. 6a). Absorbance changes of different systems for TMB as substrate been shown in 652 nm (Fig. 6b). As figure shows (Fig. 6b) the H_2O_2 + TMB + PCN-222 system presents the best absorbance change.

The experimental results showed that pH 4 and 25 °C will be the maximum catalytic activity of PCN-222(Fe). So that pH 4, T = 25 °C selected as for assay condition.

For further analysis of catalytic mechanism, peroxidase activity of PCN-222(Fe) was investigated on a certain range of chromogenic substrate. To study the kinetic parameters, the Michaelis–Menten curve was achieved and Michaelis Constant (k_m), maximum reaction velocity V_{max}, k_{cat} and k_{cat}/k_m were calculated by Lineweaver–Burk curve and Eadie–Hofstee (Fig. 7a, b).

The peroxidase activity of PCN-222(Fe) is also shown in Table 2. In this Table, the kinetic parameters of PCN-222(Fe) were compared with other nanozymes. k_m is the concentration of the substrate that the speed of reaction is equivalent to half maximum velocity. The apparent k_m value of PCN-222 (Fe) with TMB as the substrate was lower than HRP, Hemin and other catalysts, suggesting that the PCN-222(Fe) have a higher affinity for TMB than other nanozymes. The best scale for comparing the efficiency of different enzymes with together is k_{cat}/k_m. Catalytic efficiency (k_{cat}/k_m) of PCN-222(Fe) is greater than Pt NPs, Hemin and other catalyst but the value of this parameter for PCN-222(Fe) shows that the catalytic efficiency is less than the HRP. Due to high surface area of this catalyst (2200 $m^2\,g^{-1}$) most of porphyrins (active site) are available for catalytic reaction. While in the case of Hemin and other nanoparticles aggregation prevents accessibility of inner sites to react effectively.

Table 1 Comparative rate constants value for HRP and PCN-222(Fe) catalysts

Catalyst	k_1 ($M^{-1}\,s^{-1}$)	k_3 ($M^{-1}\,s^{-1}$)
PCN-222(Fe)	1.4×10^5	1.31×10^5
HRP	3.72×10^7	2.25×10^5

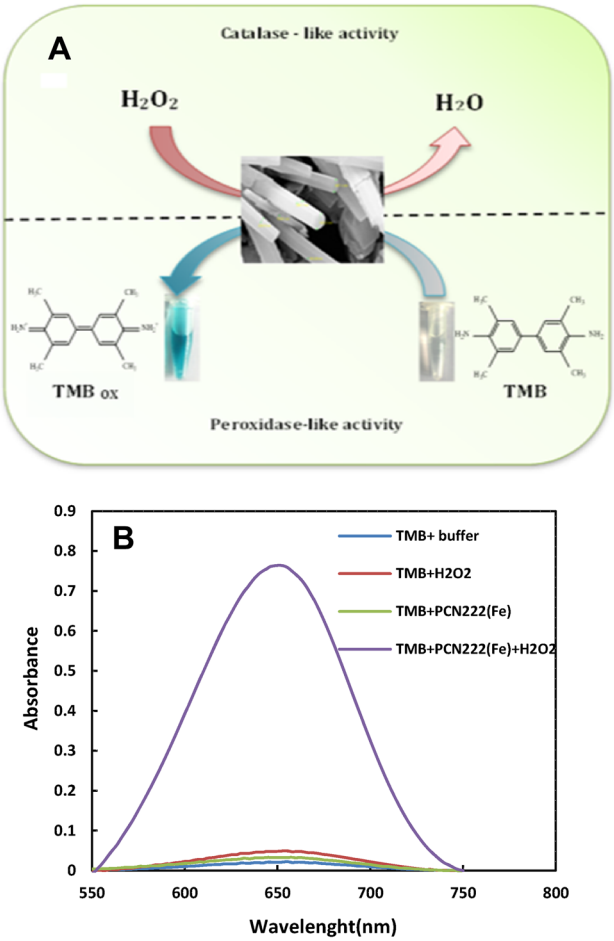

Fig. 6 **a** Corresponding reaction scheme for TMB oxidation with H_2O_2. **b** Absorbance spectra in different reaction system. Solutions in 50 mM acetate (pH 4.0) incubated and stirred at room temperature for 5 min

In order to evaluate the catalase-like activity of the prepared PCN-222(Fe), the catalytic oxidation of hydrogen peroxide in the presence of fixed concentration of substrate, TMB was tested. To obtain kinetic parameters, Michaelis–Menten, Line–Weaver–Burk and Eadie–Hofstee curves were plotted (Fig. 7c, d).

As shown in Table 2, the amount of k_{cat} that demonstrates the efficiency of the catalyst, PCN-222(Fe) is more than MMS40 and MNPs. However, the V_{max} values are equal to HRP and PCN-222(Fe). However, k_{cat} of HRP is 105 larger than of PCN-222(Fe) due to designed 3D structure of HRP as an enzyme. The kcat/km value of the PCN-222(Fe) and MMS-40 with H_2O_2 as substrate are similar. The km value of PCN-222(Fe) with H_2O_2 as the substrate is much lower than other nanoparticles, indicating PCN-222(Fe) is much more affinity to H_2O_2 which makes it a good reagent in H_2O_2 detection. Michaelis–Menten curve was achieved and Michaelis Constant (km), maximum reaction velocity Vmax, kcat and k_{cat}/k_m were calculated by Lineweaver–Burk curve and Eadie–Hofstee (Fig. 7a, b).

3.4 Sensing application of PCN-222(Fe)

Hydrogen peroxide detection is a common analysis in the clinic and industry, also this colorimetric method is simply based on intrinsic peroxidase-like property of PCN-222(Fe). A linear relationship is established in the range of 3–200 µM with a correlation coefficient of 0.9977 (Fig. 8). The detection limit of H_2O_2 was found to be about 1 µM. (Table 3). The values of these parameters, in comparison with other references, indicate that the PCN-222(Fe) is highly sensitive and selective.

The determination of H_2O_2 in real samples is important in diverse fields. It can be seen that the H_2O_2 has unique properties like stabilizing in the commercial milk but its values should be strictly controlled because the additional H_2O_2 in milk may be harm to our health. To assess the PCN-222(Fe) as sensor to detection of H_2O_2, We applied a milk sample. Results were indicated PCN-222(Fe) has the possibility and potential application in analysis of real samples (Table 4). Relative standard deviation of five repeated measurements was within the range of 1.16–1.32% that demonstrate the practicality of our proposed method for future practical application.

To further explore the function PCN-222 (Fe) as a sensor in many biochemical reactions, we applied a colorimetric method to detect of glucose. This method is based on peroxidase reaction, which is one of the best methods that has attracted many scientists due to the accuracy and simplicity for measurement of glucose. As Fig. 9 indicates by increasing glucose concentration, absorption maxima at 652 nm increase directly: firstly glucose is converted to gluconic acid and hydrogen peroxide by action of Go_x. Secondly resulting H_2O_2 oxidizes TMB in the presence of PCN-222(Fe) leading to color product of 652 nm quantitatively. So we measured the color change from TMB for determining the concentration of glucose indirectly (Fig. 9).

From analysis of dose–response curves using the PCN-222(Fe), the limit of detection (LOD) for glucose was determined to 2.2 µM in the linear range from 12 to 75 µM. lower values of this parameter for PCN-222(Fe) indicates the greater sensitivity of PCN-222-(Fe) to glucose (Table 3).

To evaluate the selectivity of this method, other carbohydrates were used and control experiments were performed under the same conditions using fructose, galactose, and maltose. As one can see in Fig. 9c, results are clearly indicating the excellent selectivity of the colorimetric bioassay for glucose.

In order to demonstrate of high sensitivity of PCN-222(Fe) in glucose detection and to confirm of its applicability in clinical diagnostics, a colorimetric assay was

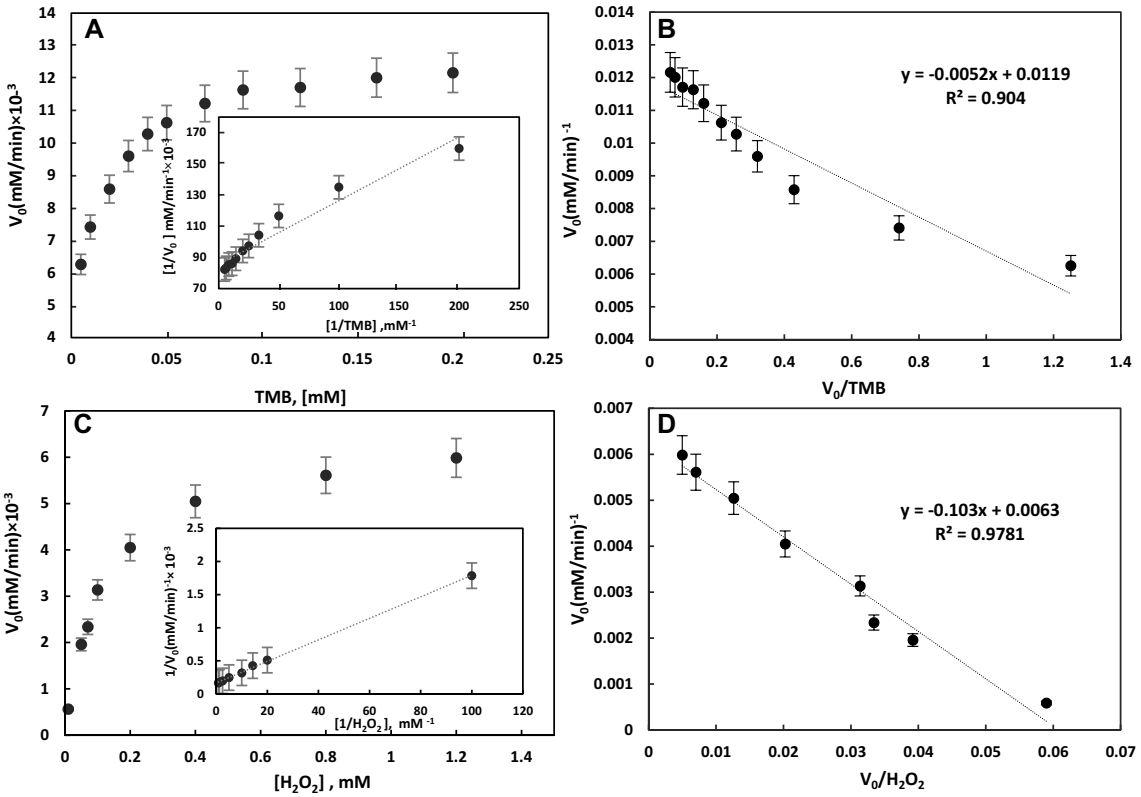

Fig. 7 Steady-state kinetic analyses using Michaelis–Menten model, Eadi-Hofstee and Lineweaver–Burk model (insets) for PCN-222(Fe). **a** and **b** Variation of TMB concentration at constant H_2O_2 concentration (0.5 mM). **c** and **d** Variation of H_2O_2 concentration at constant TMB concentration (0.2 mM). For **a** to **d**, the reaction was measured using PCN-222(Fe) in HAc-NaAc buffer (pH 4) at 25 °C

Table 2 Comparison of the apparent Kinetic data for peroxidase/catalase-like behavior study of Fe-MSN and other catalysts

Enzyme mimics	k_m (mM)	V_{max} (mM S^{-1})	k_{cat} (S^{-1})	k_{cat}/k_m (mM^{-1} S^{-1})	References
TMB					
PCN-222(Fe)	0.0048	1.88×10^{-4}	7.58×10^{-2}	1.57×10^{1}	This work
HRP	0.434	1×10^{-4}	4×10^{3}	9.21×10^{3}	[26]
Pt NPs	0.051	1.1×10^{-7}	7.1×10^{-3}	1.4×10^{-1}	[3]
Pt-Se NPs	0.029	1.9×10^{-7}	1.3×10^{-2}	4.4×10^{-1}	[3]
Hemin	0.78	-	1.6×10^{-3}	2.1×10^{-3}	[67]
MMS-40	0.193	3.33×10^{-4}	6.8×10^{-3}	3.5×10^{-2}	[68]
MNPs	0.173	1.72×10^{-4}	7.6×10^{-4}	6.8×10^{-3}	[68]
H_2O_2					
PCN-222(Fe)	0.0967	1×10^{-4}	4.01×10^{-2}	4.1×10^{-1}	This work
HRP	3.70	8.71×10^{-5}	4×10^{3}	9.4×10^{2}	[26]
MMS-40	273	4.86×10^{-1}	6.8×10^{-3}	3.6×10^{-2}	[68]
MNPs	185	2.86×10^{-1}	7.6×10^{-4}	6.8×10^{-3}	[68]

HRP Horseradish peroxidase, *MMS-40* magnetic mesoporous silica, *free MNPs* magnetic nanoparticles

developed in four human serum samples containing different concentrations of glucose. The results of sensing in serum samples were compared with the consequence of the hospital method in Table 5.

As shown in the Table 5 student t-test proved that there is no significant difference between the two methods. Also for this proposed colorimetric method, average RSD is less than 1.56% that indicate an acceptable response of our system for glucose detection.

To illustrate stability of PCN-222(Fe) as artificial peroxidase enzyme, the control experiments were carried out. This catalyst can be considered as a viable substitute

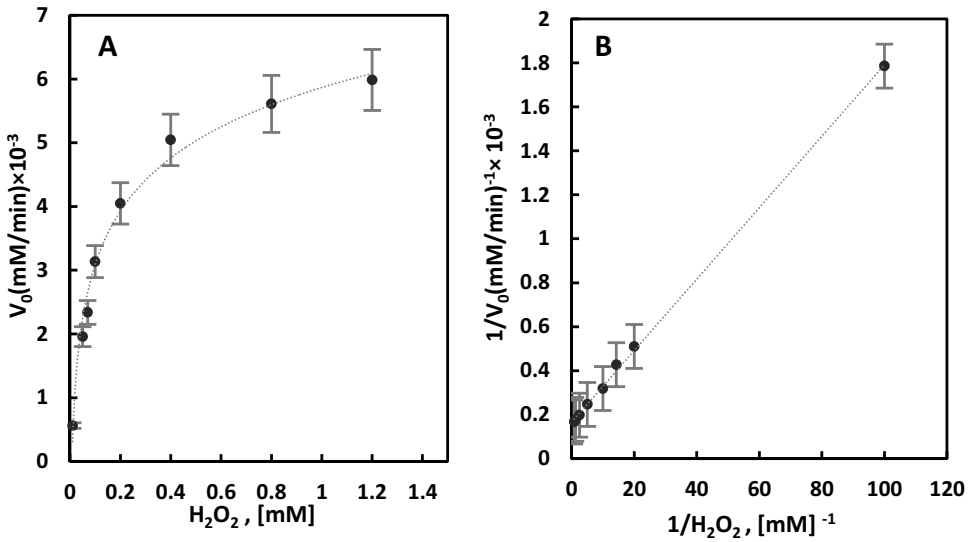

Fig. 8 **a** dose–response curve for H_2O_2 detection using PCN-222 (Fe) an artificial enzyme and **b** the linear calibration plot for H_2O_2. The error bars represent the standard deviation of three measurements Experiment condition: 2.5 µg/mL PCN-222(Fe); sodium acetate buffer (50 mM, pH 4); T = 25 °C, Reaction time 10 min

Table 3 Comparison of linear range and LOD obtained by the PCN-222(Fe) with other peroxidase mimics for H_2O_2 and glucose

Catalyst	H_2O_2		Glucose		
	Linear range (µM)	LOD (µM)	Linear range (µM)	LOD (µM)	Reference
PCN-222(Fe)	3–200	1	12–75	2.2	This work
H_2TCCP-ZnS[a]	10–60	15.8	50–500	36	[69]
MOF-808	10–1500	4.5	5.7–1700	5.7	[70]
MOF(Co/2Fe)	10–100	5	–	–	[71]
NiFe-LDHNS	10–500	4.4	50–2000	23	[72]
FePt/Go	30–500	22	–	–	[73]
Co_3O_4 NPs	50–2500	10	10–1000	5	[26]
Ce NPs	4–40	2.5	4–40	2	[74]
Co–Al LDH	10–200	10	50–500	50	[75]

[a]H_2TCPP-ZnS: porphyrin functionalized ZnS, *NiFe-LDHNS* NiFe layered double hydroxide nanosheets, *FePt/Go* FePt nanoparticles-decorated graphene oxide, *Co–Al LDHs* Co–Al layered double hydroxides

Table 4 Determination of H_2O_2 of milk samples with PCN-222(Fe)

Number	Detected (µM)	Added (µM)	Found (µM ± SD)	Recovery (%)	RSD (%)
1	ND	1	0.98 ± 0.013	98	1.32
2	ND	10	9.85 ± 0.12	98	1.22
3	ND	25	24.61 ± 0.28	98	1.16

ND No detection

for native peroxidase because the experiment proved that PCN-222(Fe) has good thermal stability at temperatures 25–60. Also, the results illustrate that the PCN-222(Fe) can also keep its high performance in the catalytic activity, over a wide pH range from 2 to 9 (Fig. 10a, b).

Additionally, to display the reusability of PCN-222(Fe) were applied the catalytic reaction successively for ten cycles that as you see in Fig. 9c there was no obvious loss in the absorbance values at 652 nm.

4 Conclusion

In this study, we investigated the multienzyme behavior of PCN-222(Fe) particles in acetate buffer solution. As a catalase mimic, it catalyzes the facile degradation of hydrogen peroxide with catalytic efficiency comparable to other similar catalysts. In presence of TMB as chromogenic substrate peroxidase-like activity was studied

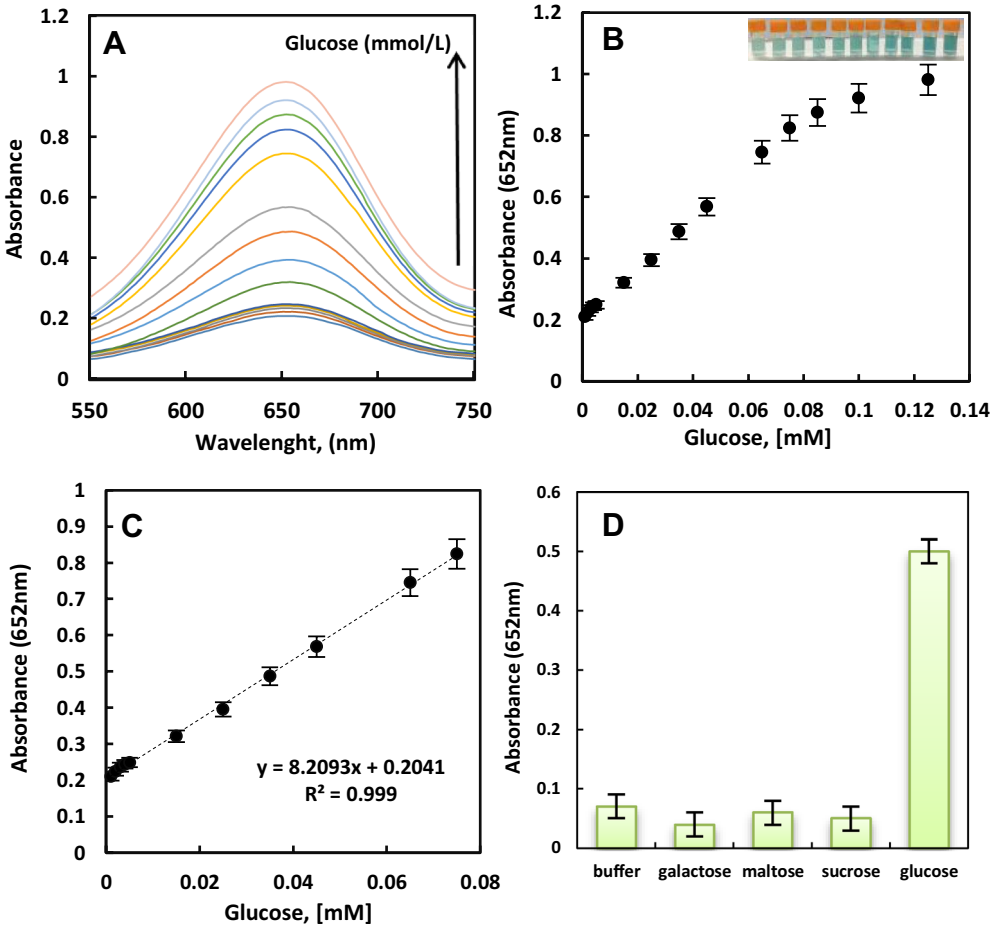

Fig. 9 **a** Absorbance variation as a result of varied glucose concentration, **b** a dose–response curve for glucose detection using PCN-222(Fe), **c** Linear calibration plot for Glucose, **d** Determination of the selectivity of glucose detection with 5 mM galactose, 5 mM maltose, 5 mM sucrose and 0.01 mM glucose

Table 5 Determination of glucose in human serum

Samples	This methods (mM ± SD) (n = 5)	Hospital methods (mM)[a]	*t* test
No. 1	4.94 ± 0.1	5.01	$1.57 < t_{0.05}$ (2.57)
No. 2	6.08 ± 0.09	6.11	$1.75 < t_{0.05}$ (2.57)
No. 3	5.46 ± 0.05	5.51	$0.89 < t_{0.05}$ (2.57)
No. 4	4.87 ± 0.09	4.92	$1.24 < t_{0.05}$ (2.57)

[a]Results obtained by BT-3000 chemistry analyzer (Biotecnica)

which showed lower k_m than other catalysts, which in turn reflects higher affinity to the substrate.

Our study provides a comparative analysis of PCN-222(Fe) as an enzyme mimic with respect to Horseradish Peroxidase and other related biocatalysts. Porous structure of the catalyst along with its robustness and stability under aqueous buffer condition resembles similar natural biocatalyst, HRP. Although catalytic efficiency of PCN-222(Fe) is lower than, it doesn't have issues of enzymes "*e.g.*, activity loss due to denaturation resulting from chemical or thermal stresses".

Owing to the unique features of PCN-222(Fe), we were designed a sensing platform for the detection of H_2O_2 and Glucose using PCN-222(Fe). As the results indicate, based on catalytic activity of PCN-222(Fe), H_2O_2 can be detected with a linear range of 3–200 µM and a detection limit (LOD) of 1 µM and glucose can be detected with a linear range of 12–75 µM and a detection limit (LOD) of 2.2 µM. The evidence collected in the sensor field has shown that PCN-222(Fe) holds great potential as a biosensor in various industries and makes it a suitable candidate for clinical purposes.

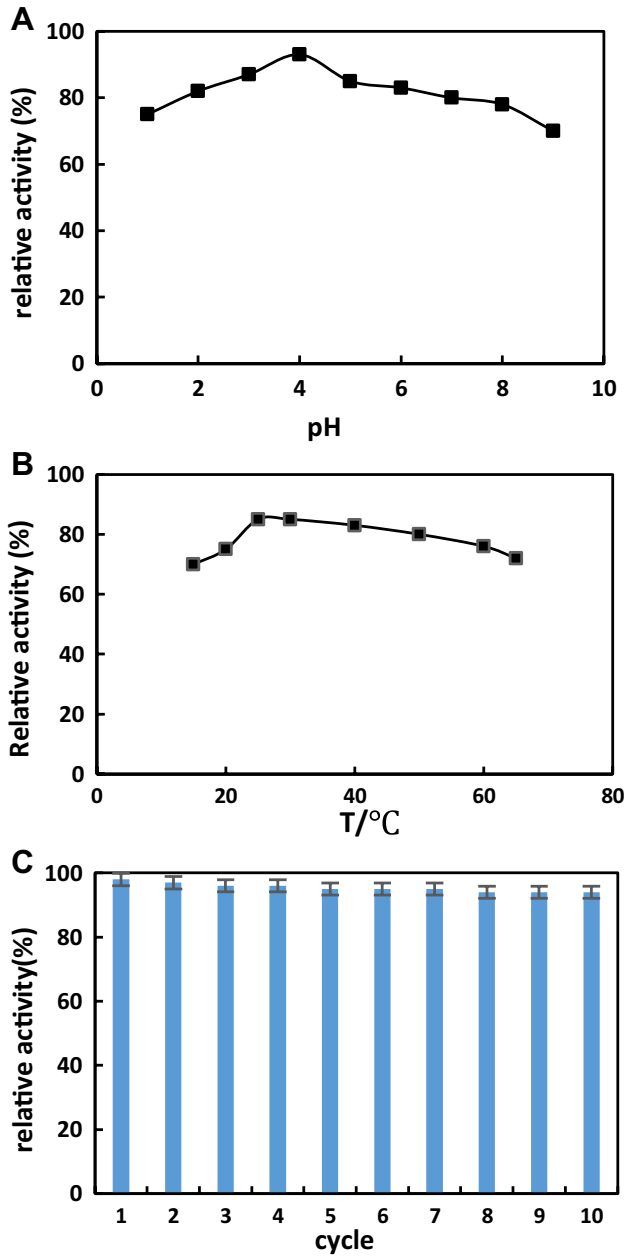

Fig. 10 The catalytic relative activity of PCN-222(Fe) is pH (**a**), Temperature (**b**), Ten PCN-222(Fe) catalytic cycles (**c**)

References

1. W.P. Lustig, S. Mukherjee, N.D. Rudd, A.V. Desai, J. Li, S.K. Ghosh, Metal–organic frameworks: functional luminescent and photonic materials for sensing applications. Chem. Soc. Rev. **46**, 3242–3285 (2017)
2. J. Kim, A.S. Cambell, J. Wang, Wearable non-invasive epidermal glucose sensors: a review. Talanta **177**, 163–170 (2018)
3. L. Guo, L. Mao, K. Huang, H. Liu, Pt–Se nanostructures with oxidase-like activity and their application in a selective colorimetric assay for mercury (II). J. Mater. Sci. **52**, 10738–10750 (2017)
4. G. Maduraiveeran, M. Sasidharan, V. Gansan, Electrochemical sensor and biosensor platforms based on advanced nanomaterials for biological and biomedical applications. Biosens. Bioelectron. **103**, 113–129 (2018)
5. F. Bibi, C. Guillaume, N. Gontard, B. Sorli, A review: RFID technology having sensing aptitudes for food industry and their contribution to tracking and monitoring of food products. Trends Food Sci. Technol. **62**, 91–103 (2017)
6. F. Qiao, L. Chen, X. Li, L. Li, S. Ai, Peroxidase-like activity of manganese selenide nanoparticles and its analytical application for visual detection of hydrogen peroxide and glucose. Sens. Actuator B-Chem. **193**, 255–262 (2014)
7. W. Chen, J. Chen, Y.B. Feng, L. Hong, Q.Y. Chen, L.F. Wu, X.H. Lin, X.H. Xia (2012) Peroxidase-like activity of water-soluble cupric oxide nanoparticles and its analytical application for detection of hydrogen peroxide and glucose. Analyst 137, 1706–1712.
8. Y. Gao, Y. Wu, J. Di, Colorimetric detection of glucose based on gold nanoparticles coupled with silver nanoparticles. Spectrochim. Acta Part A. **173**, 207–212 (2017)
9. C.L. Hsu, J.H. Lin, D.X. Hsu, S.H. Wang, S.Y. Lin, T.J. Hsueh (2017) Enhanced non-enzymatic glucose biosensor of ZnO nanowires via decorated Pt nanoparticles and illuminated with UV/green light emitting diodes. Sens. Actuators B-Chem. 238, 150–159
10. Y. Ding, M. Chen, K. Wu, M. Chen, L. Sun, Z. Liu, Z. Shi, Q. Liu, High-performance peroxidase mimics for rapid colorimetric detection of H_2O_2 and glucose derived from perylene diimides functionalized Co_3O_4 nanoparticles. Mater. Sci. Eng. C. **80**, 558–565 (2017)
11. Z. Zhao, Q. Ou, X. Yin, J. Liu. Nanomaterial-based electrochemical hydrogen peroxide biosensor. Int. J. Biosens. Bioelectron. **2**, 25–28 (2017)
12. Q. Liu, Y. Yang, X. Lv, Y. Ding, Y. Zhang, J. Jing, C. Xu, One-step synthesis of uniform nanoparticles of porphyrin functionalized ceria with promising peroxidase mimetics for H_2O_2 and glucose colorimetric detection. Sens. Actuator B-Chem **240**, 726–734 (2017)
13. L.C. Clark, C. Lyons, Electrode systems for continuous monitoring in cardiovascular surgery. Ann. N.Y. Acad. Sci. **102**, 29–45 (1962)
14. V. Cerda, A. Gonzalez, K. Danchana, From thermometric to spectrophotometric kinetic-catalytic methods of analysis: a review. Talanta **167**, 733–746 (2017)
15. M. Liu, R. Liu, W. Chen, Graphene wrapped Cu_2O nanocubes: non-enzymatic electrochemical sensors for the detection of glucose and hydrogen peroxide with enhanced stability. Biosens. Bioelectron. **45**, 206–212 (2013)
16. W. Li, D. Qian, Q. Wang, Y. Li, N. Bao, H. Gu, C. Yu, Fully-drawn origami paper analytical device for electrochemical detection of glucose. Sens. Actuators B-Chem. 231, 230–238 (2016)
17. C. Shen, J. Su, X. Li, J. Luo, M. Yang, Electrochemical sensing platform based on Pd–Au bimetallic cluster for non-enzymatic detection of glucose. Sens. Actuators B-Chem. **209**, 695–700 (2015)
18. F. Wang, Q. Hao, Y. Zhang, Y. Xu, W. Lei, Fluorescence quenchometric method for determination of ferric ion using boron-doped carbon dots. Microchim. Acta 183, 273–279 (2016).
19. Z. Yang, Z. Zhang, Y. Jiang, M. Chi, G. Nie, X. Lu, C. Wang, Palladium nanoparticles modified electrospun $CoFe_2O_4$ nanotubes with enhanced peroxidase-like activity for colorimetric detection of hydrogen peroxide. RSC Adv. **6**, 33636–33642 (2016)
20. R.J. Russell, M.V. Pishko, C.C. Gefrides, M.J. McShane, G.L. Cote, A fluorescence-based glucose biosensor using concanavalin A and dextran encapsulated in a poly (ethylene glycol) hydrogel. Anal. Chem. 71, 3126–3132 (1999).
21. P.H. Hynninen, V. Kaartinen, E. Kolehmainen, Horseradish peroxidase-catalyzed oxidation of chlorophyll a with hydrogen

peroxide: characterization of the products and mechanism of the reaction. Biochim. Biophys. Acta **1797**, 531–542 (2010)
22. S. Dong, L. Mao, S. Luo, L. Zhou, Y. Feng, S. Gao. Comparison of lignin peroxidase and horseradish peroxidase for catalyzing the removal of nonylphenol from water. Environ. Sci. Pollut. Res. Int. **21**, 2358–2366 (2014)
23. S.B. Maddinedi, B.K. Mandal, Peroxidase like activity of quinic acid stabilized copper oxide nanosheets. Austin J. Anal. Pharm. Chem. **1**, 1–4 (2014)
24. L. Gao, J. Zhuang, L. Nie, J. Zhang, Y. Zhang, N. Gu, T. Wang, J. Feng, D. Yang, S. Perrett, X. Yan, Intrinsic peroxidase-like activity of ferromagnetic nanoparticles. Nat. Nanotechnol. 2, 577–583 (2007).
25. H. Wei, E. Wang, Nanomaterials with enzyme-like characteristics (nanozymes): next-generation artificial enzymes. Chem. Soc. Rev. **42**, 6060–6093 (2013)
26. J. Mu, Y. Wang, M. Zhao, L. Zhang, Intrinsic peroxidase-like activity and catalase-like activity of Co_3O_4 nanoparticles. Chem. Commun. **48**, 2540–2542 (2012)
27. R. Andre, F. Natalio, M. Humanes, J. Leppin, K. Heinze, R. Wever, H.C. Schroeder, W.E.G. Mueller, W. Tremel, V_2O_5 Nanowires with an intrinsic peroxidase-like activity. Adv. Funct. Mater. **21**, 501–509 (2011)
28. S.K. Maji, A.K. Dutta, P. Biswas, D.N. Srivastava, P. Paul, A. Mondal, B. Adhikary, Synthesis and characterization of FeS nanoparticles obtained from a dithiocarboxylate precursor complex and their photocatalytic, electrocatalytic and biomimic. Appl. Catal. A-Gen. **419**, 170–177 (2012)
29. Y. Song, K. Qu, C. Zhao, J. Ren, X. Qu, Graphene oxide: intrinsic peroxidase catalytic activity and its application to glucose detection. Adv. Mater. **22**, 2206–2210 (2010)
30. W. Shi, Q. Wang, Y. Long, Z. Cheng, S. Chen, H. Zheng, Y. Huang, Carbon nanodots as peroxidase mimetics and their applications to glucose detection. Chem. Commun. **47**, 6695–6697 (2011)
31. J.W. Zhang, H.T. Zhang, Z.Y. Du, X. Wang, S.H. Yu, H.L. Jiang, Water-stable metal–organic frameworks with intrinsic peroxidase-like catalytic activity as a colorimetric biosensing platform. Chem. Commun. **50**, 1092–1094 (2014)
32. Y. Bai, Y. Dou, L.H. Xie, W. Rutledge, J.R. Li, H.C. Zhou, Zr-based metal–organic frameworks: design, synthesis, structure, and applications. Chem. Soc. Rev. **45**, 2327–2367 (2016)
33. H. Deng, S. Grunder, K.E. Cordova, C. Valente, H. Furukawa, M. Hmadeh, F. Gándara, A.C. Whalley, Z. Liu, S. Asahina, Large-pore apertures in a series of metal-organic frameworks. Science **336**, 1018–1023 (2012)
34. M.D. Allendorf, V. Stavila, Crystal engineering, structure–function relationships, and the future of metal–organic frameworks. CrysEngCommun **17**, 229–246 (2015)
35. D. Sun, W. Liu, M. Qiu, Y. Zhang, Z. Li, Introduction of a mediator for enhancing photocatalytic performance via post-synthetic metal exchange in metal–organic frameworks (MOFs). Chem. Commun. **51**, 2056–2059 (2015)
36. W. Morris, B. Volosskiy, S. Demir, F. Gandara, P.L. McGrier., H. Furukawa, D. Cascio, J.F. Stoddart, O.M. Yaghi, Synthesis, structure, and metalation of two new highly porous zirconium metal–organic frameworks. Inorg. Chem. **51**, 6443–6445 (2012)
37. Y. Chen, T. Hoang, S. Ma, Biomimetic catalysis of a porous iron-based metal–metalloporphyrin framework. Inorg. Chem. **51**, 12600–12602 (2012)
38. X.S. Wang, M. Chrzanowski, D. Yuan, B.S. Sweeting, S. Ma, Covalent heme framework as a highly active heterogeneous biomimetic oxidation catalyst. Chem. Mater, 26, 1639–1644 (2014).
39. L. Ai, L. Li, C. Zhang, J. Fu, J. Jiang, MIL-53 (Fe): a metal–organic framework with intrinsic peroxidase-like catalytic activity for colorimetric biosensing. Chem.–Eur. J **19**, 15105–15108 (2013)
40. H. Yu, D. Long, Highly chemiluminescent metal-organic framework of type MIL-101 (Cr) for detection of hydrogen peroxide and pyrophosphate ions. Microchim. Acta., 183, 3151–3157 (2016).
41. K. Wang, D. Feng, T.F. Liu, J. Su, S. Yuan, Y.P. Chen, M. Bosch, X. Zou, H.C. Zhou, A series of highly stable mesoporous metalloporphyrin Fe-MOFs. J. Am. Chem. Soc. **136**, 13983–13986 (2014)
42. D. Feng, W.C. Chung, Z. Wei, Z.Y. Gu, H.L. Jiang, Y.P. Chen, D.J. Darensbourg, H.C. Zhou, Construction of ultrastable porphyrin Zr metal–organic frameworks through linker elimination. J. Am. Chem. Soc. **135**, 17105–17110 (2013)
43. D. Feng, Z.Y. Gu, J.R. Li, H.L. Jiang, Z. Wei, H.C. Zhou, Zirconium-metalloporphyrin PCN-222: mesoporous metal–organic frameworks with ultrahigh stability as biomimetic catalysts. Angew. Chem. Int. Ed. **51**, 10307–10310 (2012)
44. P.G. Rodríguez, C.F. Batista, R. Vazquez-Duhalt, B. Valderrama. A novel heme peroxidase from *Raphanus sativus* intrinsically resistant to hydrogen peroxide. Eng. Life Sci. **8**, 286–296 (2008)
45. A.J. Howarth, Y. Liu, J.T. Hupp, O.K. Farha, Metal–organic frameworks for applications in remediation of oxyanion/cation-contaminated water. Crys Eng Comm. **17**, 7245–7253 (2015)
46. Z.Y. Gu, J. Park, A. Raiff, Z. Wei, H.C. Zhou, Metal–organic frameworks as biomimetic catalysts. Chem Cat Chem. **6**, 67–75 (2014)
47. D.G. Blackmond, Reaction progress kinetic analysis: a powerful methodology for mechanistic studies of complex catalytic reactions. Angew. Chem., Int. Ed. **44**, 4302–4320 (2005)
48. B.H.J. Hostee, Non-Inverted Versus Inverted Plots in Enzyme Kinetics. Nature **184**, 1296–1298 (1959)
49. S. Kumari, B. Dhar, C. Panda, A. Meena, S. Gupta, Fe-TAML encapsulated inside mesoporous silica nanoparticles as peroxidase mimic: femtomolar protein detection. ACS Appl. Mater. Interfaces **6**, 13866–13873 (2014)
50. E. Austin, M. Gouterman, Porphyrins XXXVII. Absorption and emission of weak complexes with acids, bases, and salts. Bioinorg. Chem. **9**, 281–298 (1978)
51. S. Gawande, S.R. Thakare, Ternary polymer composite of graphene, carbon nitride, and poly (3-hexylthiophene): an efficient photocatalyst. Chem Cat Chem **4**, 1759–1763 (2012)
52. E.Y. Choi, T.H. Han, J. Hong, J.E. Kim, S.H. Lee, H.W. Kim, S.O. Kim, Noncovalent functionalization of graphene with end-functional polymers. J. Mater. Chem. **20**, 1907–1912 (2010)
53. X.L. Lv, K. Wang, B. Wang, J. Su, X. Zou, Y. Xie, J.R. Li, H.C. Zhou, A base-resistant metalloporphyrin metal–organic framework for C–H bond halogenation. J. Am. Chem. Soc. **139**, 211–217 (2017)
54. S. Sohrabi, S. Dehghanpour, M. Ghalekhani, A cobalt porphyrin-based metal organic framework/multi-walled carbon nanotube composite electrocatalyst for oxygen reduction and evolution reactions. J. Mater. Sci. **53**, 3624–3639 (2018)
55. Y. Yu, P. Ju, D. Zhang, X. Han, X. Yin, L. Zheng, C. Sun, Peroxidase-like activity of $FeVO_4$ nanobelts and its analytical application for optical detection of hydrogen peroxide. Sens. Actuator B-Chem **233**, 162–172 (2016)
56. K. Nazari, S. Shokrollahzadeh, A. Mahmoudi, F. Mesbahi, N. Seyed Matin, A.A. Moosavi-Movahedi, Iron (III) protoporphyrin/MCM41 catalyst as a peroxidase enzyme model: preparation and typical test reactions. J. Mol. Catal. A Chem. **239**, 1–9 (2005)
57. N.C. Veitch, Horseradish peroxidase: a modern view of a classic enzyme. Phytochemistry **65**, 249–259 (2004)
58. K. Nazari, A. Mahmoudi, R. Khodafarin, A.A. Moosavi Movahedi, A. Mohebi, Stabilizing and suicide-peroxide protecting

effect of Ni^{2+} on horseradish peroxidase. J. Iran. Chem. Soc. **2**, 232–237 (2005)
59. A. Claiborne, I. Fridovich, Chemical and enzymic intermediates in the peroxidation of o-dianisidine by horseradish peroxidase. 1. Spectral properties of the products of dianisidine oxidation. Biochemistry **18**, 2324–2329 (1979)
60. A. Mahmoudi, K. Nazari, A.A. Moosavi-Movahedi, A.A. Saboury, Enthalpy analysis of horseradish peroxidase in the presence of Ni^{2+}: a stabilization study. Thermochim. Acta **385**, 33–39 (2002)
61. Y. Liu, M. Yuan, L. Guo, R. Qiao, An efficient colorimetric biosensor for glucose based on peroxidase-like protein-Fe_3O_4 and glucose oxidase nanocomposites. Biosens. Bioelectron. **52**, 391–396 (2014)
62. A. Mahmoudi, K. Nazari, N. Mohammadian, A.A. Moosavi-Movahedi, Effect of Mn^{2+}, Co^{2+}, Ni^{2+}, and Cu^{2+} on horseradish peroxidase. Appl. Biochem. Biotechnol. **104**, 81–94 (2003)
63. J. Shu, Z.L. Qiu, Q.H. Wei, J.Y. Zhuang, D.P. Tang, Cobalt-porphyrin-platinum-functionalized reduced graphene oxide hybrid nanostructures: a novel peroxidase mimetic system for improved electrochemical immunoassay. Sci. Rep **5**, 15113 (2015)
64. M. Khosraneh, A. Mahmoudi, H. Rahimi, K. Nazari, A.A. Moosavi-Movahedi, Suicide-Peroxide inactivation of microperoxidase-11: a kinetic study. J. Enzyme Inhibit. Med. Chem. **22**, 677–684 (2007)
65. X. Wang, K. Qu, B. Xu, J. Ren, X. Qu, Multicolor luminescent carbon nanoparticles: synthesis, supramolecular assembly with porphyrin, intrinsic peroxidase-like catalytic activity and applications. Nano Research **4**, 908–920 (2011)
66. Y. Sun, H.C. Zhou, Recent progress in the synthesis of metal–organic frameworks. Sci. Technol. Adv. Mater. **16**, 054202 (2015)
67. D. Metelista, O. Rus, A. Puchkaev, Russ, Heme-containing hydroperoxide test systems for inhibitors of free-radical reactions. J. Appl. Chem. **70**, 1629–1636 (1997)
68. M. Kim, J. Shim, T. Li, J. Lee, H. Park, Fabrication of nanoporous nanocomposites entrapping Fe_3O_4 magnetic nanoparticles and oxidases for colorimetric biosensing. Chem. Eur. J. 17, 10700–10707 (2011)
69. Q. Liu, P. Chen, Z. Xu, M. Chen, Y. Ding, K. Yue, J. Xu, A facile strategy to prepare porphyrin functionalized ZnS nanoparticles and their peroxidase-like catalytic activity for colorimetric sensor of hydrogen peroxide and glucose. Sens. Actuator B-Chem. **251**, 339–348 (2017)
70. H.Q. Zheng, C.Y. Liu, X.Y. Zeng, J. Chen, J. Lu, R.G. Lin, R. Cao, Z.J. Lin, J.W. Su, MOF-808: a metal–organic framework with intrinsic peroxidase-like catalytic activity at neutral pH for colorimetric biosensing. Inorg. Chem. **57**, 9096–9104 (2018)
71. H. Yang, R. Yang, P. Zhang, Y. Qin, T. Chen, F. Ye, A bimetallic (Co/2Fe) metal-organic framework with oxidase and peroxidase mimicking activity for colorimetric detection of hydrogen peroxide. Microchim. Acta **184**, 4629–4635 (2017)
72. T. Zhan, J. Kang, X. Li, L. Pan, G. Li, W. Hou, NiFe layered double hydroxide nanosheets as an efficiently mimic enzyme for colorimetric determination of glucose and H_2O_2. Sens. Actuator B-Chem **255**, 2635–2642 (2017)
73. M. Chen, B. Yang, J. Zhu, H. Liu, X. Zhang, X. Zheng, FePt nanoparticles-decorated graphene oxide nanosheets as enhanced peroxidase mimics for sensitive response to H_2O_2. Mater. Sci. Eng. C. **90**, 610–620 (2018)
74. R. Guo, Y. Wang, S. Yu, W. Zhu, F. Zheng, W. Liu, D. Zhang, J. Wang, Dual role of hydrogen peroxide on the oxidase-like activity of nanoceria and its application for colorimetric hydrogen peroxide and glucose sensing. RSC. Adv. **6**, 577–583 (2016)
75. L. Chen, B. Sun, X. Wang, F. Qiao, S. Ai, 2D ultrathin nanosheets of Co–Al layered double hydroxides prepared in L-asparagine solution: enhanced peroxidase-like activity and colorimetric detection of glucose. J. Mater. Chem. B. **1**, 2268–2274 (2013)